Available online at www.sciencedirect.com

jmr&t Journal of Materials Research and Technology

journal homepage: www.elsevier.com/locate/jmrt

Review Article

Microstructure and electrical contact behavior of Al_2O_3–Cu/30W3SiC(0.5Y_2O_3) composites

Xianhua Zheng [a], Meng Zhou [a,b,c,**], Yi Zhang [a,b,c,*], Jinliang Huang [a,b,c], Yunzhang Li [a], Hanjing Zhu [a], Shunlong Tang [a], De Li [a], Shengli Liang [a], Baohong Tian [a,b,c], Yong Liu [a,b,c], Xu Li [d], Yanlin Jia [e], Alex A. Volinsky [f]

[a] School of Materials Science and Engineering, Henan University of Science and Technology, Luoyang 471023, PR China

[b] Provincial and Ministerial Co-construction of Collaborative Innovation Center for Non-ferrous Metals New Materials and Advanced Processing Technology, Henan Province, Luoyang 471023, PR China

[c] Henan Province Key Laboratory of Nonferrous Materials Science and Processing Technology, Luoyang 471023, PR China

[d] Center for Advanced Measurement Science, National Institute of Metrology, Beijing 100029, PR China

[e] College of Materials Science and Engineering, Central South University, Changsha, 410083, PR China

[f] Department of Mechanical Engineering, University of South Florida, 4202 E. Fowler Ave. ENG 030, Tampa, 33620, USA

ARTICLE INFO

Article history:
Received 1 November 2022
Accepted 12 December 2022
Available online 20 December 2022

Keywords:
Copper matrix composites
Rapid hot-pressing sintering
Internal oxidation
Electrical contact
Arc duration
Welding force

ABSTRACT

The aim of this study is to observe the organization and properties of Al_2O_3–Cu/WSiC–Y_2O_3 composites and to investigate the effect of Y_2O_3 incorporation on the electrical contact properties of the composites. Preparation of Al_2O_3–Cu/30W3SiC(0.5Y_2O_3) composites by rapid hot-pressing sintering technique. The conductivity of the composites is 59.3 %IACS and 58.3 %IACS, respectively. Hardness is 179 HV and 183 HV, respectively. Thermal conductivity is 108 W/(m·k) and 275 W/(m·k), respectively. The dense structure of the composites and the homogeneous distribution of reinforcing phases give the composites excellent overall performance. The addition of Y_2O_3 increases the resistance of the materials to arc erosion. The amount of material transfer and loss is significantly reduced, and the arc ablation phenomenon is reduced. The arc duration was significantly reduced from 4.48 ms to 0.44 ms, 5.72 ms–4.68 ms, 6.23 ms–5.52 ms, and 12.5 ms–8.59 ms, respectively; and the melt force was significantly reduced to 58.9%, 81.4%, 87.5%, and 89.4% of the original.

* Corresponding author. School of Materials Science and Engineering, Henan University of Science and Technology, Luoyang 471023, PR China.

** Corresponding author. Provincial and Ministerial Co-construction of Collaborative Innovation Center for Non-ferrous Metals New Materials and Advanced Processing Technology, Henan Province, Luoyang 471023, PR China.

E-mail addresses: zhoumeng0902@126.com (M. Zhou), zhshgu436@163.com (Y. Zhang).

https://doi.org/10.1016/j.jmrt.2022.12.071

1. Introduction

Electrical contacts are significant components of high-voltage circuit breakers, contacts, and electrical line protectors. The performance of electrical contacts directly affects the quality and service life of electrical components and is closely related to the reliability of power systems [1,2]. With the development of science and technology and production improvement, it is important to develop electrical contact materials with better performance. Combining excellent properties and synergistic strengthening mechanisms of multiple materials is commonly used for new materials design and development.

Metal matrix composites are new materials that take two or more materials and combine them by physical or chemical methods to obtain excellent properties, thus meeting the increasing performance. Compared with metals, the performance of metal matrix composites is much better [3–7]. The common methods for the preparation of metal matrix composites include spark plasma sintering (SPS) [8], powder metallurgy [9], magnetron sputtering [10], stir casting [11], hot extrusion [12], hot isostatic pressing [13], and in situ growth [14]. Copper is widely used in aerospace and electronics industries due to its excellent electrical, thermal, and machining properties. Copper matrix composites have been gradually replacing silver matrix composites and other electrical contact materials [15–17]. Dispersion-strengthened copper matrix composites have excellent comprehensive mechanical properties. In recent years, many researchers have studied the types and strengthening mechanism of dispersion-strengthened copper matrix electrical contact materials, including Al_2O_3, Y_2O_3, and Cr_2O_3 as dispersion phases [18–21], which provide remarkable strengthening effects. For example, Tian et al. [22] prepared nano-dispersed Al_2O_3 copper matrix composite by internal oxidation. The softening temperature of Cu-0.5 vol% Al_2O_3 composite obtained by internal oxidation reached 600 °C and the electrical conductivity reached 93% IACS, compared with pure copper, with significantly improved yield strength and tensile strength. Through the study of the strengthening mechanisms, it was found that nano Al_2O_3 inhibits recrystallization by napping grain boundaries and subgrain boundaries with high-density dislocations, strengthening the matrix. Zhou et al. [23] prepared a Cu–Al_2O_3 composite by a novel method of in-situ reaction synthesis at liquidus temperature. The obtained composite had superior mechanical properties, tensile strength, yield strength, Rockwell hardness, and electrical conductivity. Zhang et al. [24] prepared copper matrix composites by vacuum hot-pressing sintering and internal oxidation. The dislocation entanglement was caused by the Al_2O_3 nanoparticles pinning. The arc erosion morphology was affected by W content, the fusion welding force decreased with W content, the arc burning time was shortened, and the welding resistance was improved. Mu et al. [25] studied the effects of the Y_2O_3 content on the properties of copper-based electrical contact materials. The hardness and density of the samples increased with the Y_2O_3 content when an appropriate amount of Y_2O_3 was added. The addition of Y_2O_3 is beneficial to hinder the growth of copper particles. Due to the grain size refinement, the distribution of Y_2O_3 in the matrix was more uniform, which improved electrical properties. Compared with traditional electrical contact materials, the contact resistance of the samples containing Y_2O_3 was lower. Li et al. [26] studied the effects of Y_2O_3 content on the mechanical properties and microstructure of the W–Ni–Cu–Y_2O_3 alloy processed by cold pressing and sintering. The increase of Y_2O_3 content refined the alloy grains. When Y_2O_3 content increased to 0.5%, W grains began to grow and the porosity of the alloy increased. The density and mechanical properties of the alloy were enhanced with the Y_2O_3 addition.

It was found that introduction of SiC, WC, TiC, and other hard ceramic particles can significantly improve the hardness and friction resistance of composite materials [27–31]. Akbarpour et al. [32] investigated the effect of different sizes of SiC on the wear resistance of Cu–SiC composites. Found that the mixed-size material has higher wear resistance, lower friction coefficient and higher strength compared to single-size composites. Delamination wear is the main wear mechanism of the material. Zhang et al. [33] added SiC particles using hot pressing sintering to improve the service life of the copper matrix electrical contact materials. To improve the service life of electrical contacts with copper matrix, the continuous copper film was sputtered over β-SiC powder, improving the interfacial wettability between silicon carbide powder and copper matrix. Palma et al. [34] studied the creep behavior of the Cu-2 vol% TiC alloy and found that the activation energy of the alloy prepared by reaction and milling was 109 kJ/mol and 156 kJ/mol, respectively, and the corresponding stress index of the material was 3.1 and 6.3. Li et al. [35] studied the effects of SiC nanoparticles on the properties and solid solution behavior of 1 wt% nano-SiCp/Al–Cu composites and found that SiC showed excellent mechanical properties at a higher solution temperature, and the tensile strength and yield strength of the materials were increased by 16.3% and 34.6%, respectively. Deshpande et al. [36] prepared WC particles-reinforced Cu/W composite by infrared osmotic technology. The volume fraction of WC was 53%, the density of the material reached 99.9%, and the microhardness was between 360 HV and 370 HV. The wear resistance of the material was much better than an ordinary Cu/W composite.

W has a high melting point and is insoluble in Cu. The Cu–W composites have high hardness, good high-temperature performance, wear and corrosion resistance, and have been utilized in aerospace, industrial metallurgy, and other fields [37,38]. W can enhance the high-temperature performance of Cu alloys or copper matrix composites and is an ideal reinforcing phase for electrical contact materials [39,40]. Amalu et al. [41] used SPS to produce tungsten-copper and molybdenum-copper composite materials. Compared with traditional liquid phase sintering and osmosis technology, the electrical conductivity of the samples prepared by SPS was significantly higher than by other methods, and the densification was very high with 99.1–100% relative density. Zhuo et al. [42] used spherical initial powder to prepare Cu/W alloys through continuous processes such as powder mixing, cold pressing, sintering, and infiltration. Compared with other commercial alloys, the hardness of the synthesized Cu/W composite was increased by 7.3%, electrical conductivity by 23.3%, and strain by 8.8%. Huang et al. [43] studied the creep, friction, and wear behavior of WCu pseudo-alloy at

high temperatures, and observed that the Cu phase was evenly distributed around the W skeleton. The WCu alloy creep resistance decreased with lower W content while increasing Cu content helped to enhance the cohesion of the W–Cu phase and improved the deformation capacity of W. The friction coefficient decreased with Cu content and applied load. Han et al. [44] developed ultra-fine grain Cu/W composite materials with 1200 MPa compressive strength, 48.6% IACS electrical conductivity, and 357 HV microhardness. The grain refinement, dislocation hindrance, and stress transfer are the main strengthening mechanisms. Peng et al. [45] studied the deformation mechanism, relative density, and uniformity of Cu/W composite powder under quasi-static compression by using the multi-particle finite element method. Wang et al. [46] designed a porous W structure on the surface of copper by osmotic method and prepared a new type of CuW/Al composite material. The effects of temperature and holding time on the microstructure of the interface were studied. Hiraoka et al. [47] observed the microstructure evolution and deformation behavior of the W-80 vol% Cu composite. The deformation of W particles was small, and the porosity of the composite decreased after deformation.

When designing the composition of the material, we synthesized the existing studies and found that reinforcing phases such as W, SiC, Al_2O_3 and Y_2O_3 were added to the Cu matrix. The incorporation of W gives the composite excellent high temperature properties. The introduction of W phase in Cu resulted in excellent performance of the material in terms of mechanical properties and resistance to arc erosion. The SiC ceramic phase has good chemical stability. Cu–SiC composites can significantly increase the mechanical properties of the material, such as high strength, good wear resistance, low coefficient of thermal expansion and significant high temperature properties. Al_2O_3 particles have high hardness. In the copper matrix, Al_2O_3 exhibits chemical inertness and thermodynamic stability. It can hinder the slip of dislocations in the copper matrix, thus strengthening the copper matrix. The dispersive copper matrix composites with Al_2O_3 as the reinforcing phase have excellent overall performance. Y_2O_3 can refine Cu matrix grains. It improves the wettability of Cu and enhances the electrical contact properties of Cu matrix composites.

In this work, we combined the advantages of some of the above-mentioned reinforcing phases. Cu was used as the matrix, Al_2O_3、W and SiC were used to improve the high temperature mechanical properties of the composites, and Y_2O_3 was used to improve the arc erosion resistance to design the Al_2O_3–Cu/WSiC–Y_2O_3 composites. The aim of this study is to synthesize the synergistic strengthening effects of various strengthening phases. To investigate the structure properties and microstructure of Al_2O_3–Cu/WSiC–Y_2O_3 composites. To investigate the electrical contact properties of the materials, especially the effect of Y_2O_3 on the electrical contact properties of copper matrix composites. Develop a copper matrix composite with excellent overall performance and good resistance to arc erosion. Cater to the trend of silver saving or silver substitution in the field of electric contact materials, and contribute to the development of copper-based electric contact composites.

2. Experiments

2.1. Preparation and characterization of composites

Starting materials were Cu-0.2 A l alloy powder (purity≥99.9%, mean particle size≤38 μm); W powder (purity≥99.95%, mean particle size≤5 μm); SiC powder (purity≥99.95%, average particle size: 3–5 μm); Cu_2O powder (purity≥99.95%, mean particle size: 2–5 μm); Y_2O_3 nano-powder (purity≥99.99%, average particle size≤5 nm). In the sintering process, Cu_2O provides an oxygen source, and the nano Al_2O_3 dispersion-reinforced copper matrix was produced by the internal oxidation method, where W, SiC, and Y_2O_3 particles further strengthen the matrix. Fig. 1 shows the morphology characterization of the original powder by using a JSM-5610 L V scanning electron microscope.

The desired powder was weighed and placed into a homemade ball mill. To avoid the contamination of the alloy powder during the ball milling process, homemade plastic ball milling tanks were used. In addition, pure copper balls were used as ball milling media with a ball-to-material ratio of 4:1. After the powder and ball milling media were loaded, the jar was sealed and placed in the QQM/B light-duty ball mill for 6 h. After mixing, the alloy powder was placed into a graphite mold with an inner diameter of 30 mm, and the powder was vacuum sintered in the FHP-828 fast hot-pressing sintering furnace. After the vacuum degree was reduced to 0 Pa, the mold temperature was raised to 700 °C for 5 min, the axial contact pressure was increased to 45 MPa, and the alloy powder was heated to 900 °C for 1 min. Then the mold was heated to 950 °C and kept for 10 min. During the sintering heating process, the pressure was maintained at 45 MPa and the heating rate was 100 °C/min. After 9 min the temperature and pressure of the mold were reduced to 500 °C and 30 MPa, respectively. After the mold was cooled to room temperature, composites were taken out. The composite samples were wire cut to the specified dimensions according to the subsequent experimental requirements. Fig. 2 shows a schematic diagram of the composite preparation process.

2.2. Material performance testing and characterization

To test the properties of the sintered composite samples, sandpaper is used to polish the sintered samples smoothly before the measurement to reduce the experimental error. The conductivity of the sample is measured using a Sigma 2008B1 conductivity meter. 8 areas are selected on the surface of the sintered sample and the conductivity is measured and averaged. The density of the sample is measured by Archimedes method using MS304S density meter, and the average value is taken after 5 measurements for each sample. Using HV-100 Vickers hardness tester to measure the hardness of the sample, 7 different areas are selected on the surface of the sample and the hardness of the sample is measured separately, and the sample hardness is averaged. The thermal conductivity values of the materials are measured using the LFA 457 MicoFlash Thermal Conductivity Analyzer at 150 °C. Each sample is measured three times and the results are averaged. X-ray diffraction (XRD) of D8-ADVANCE with Cu

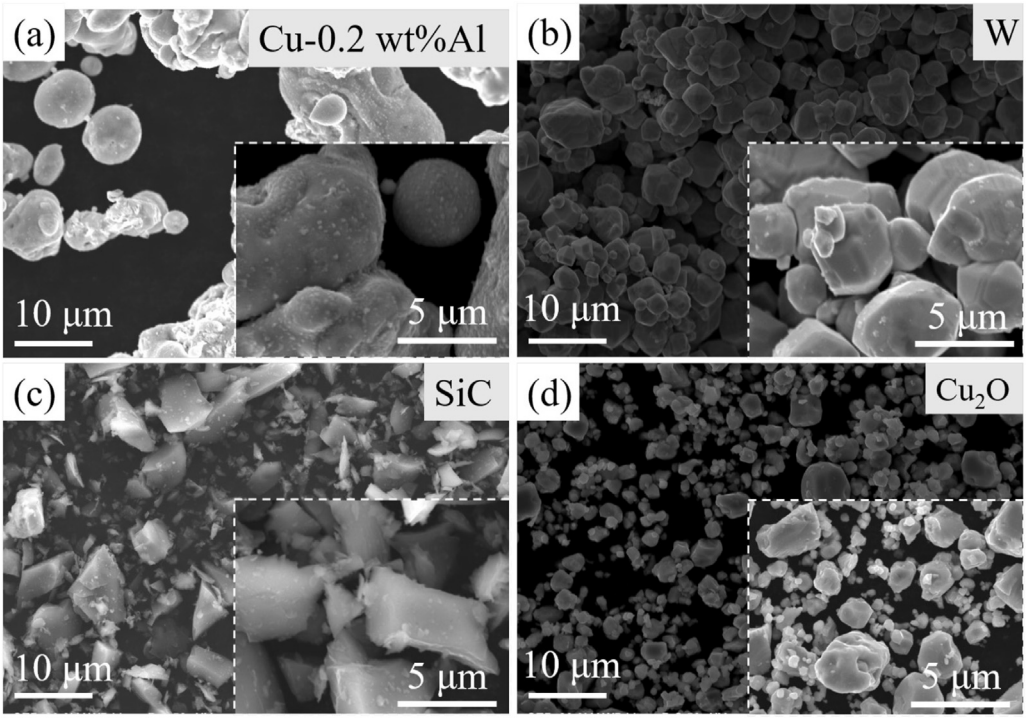

Fig. 1 – Morphology of the original powders: (a) Cu-0.2 wt% Al; (b) W; (c) SiC; (d) Cu_2O.

target as X-ray emitter was used for the physical phase analysis of the sample, with a scan rate of 6o/min and a scan range of 15°-90°. Using an electric thermostatic chamber furnace, the specimens were charged at a constant temperature of 150 °C for oxidation performance testing, with an oxidation time of 20 h. Analysis and determination of sample microstructure and element distribution using JSM-7800 F scanning electron microscope (SEM). The sample microstructure was analyzed using a FEI Tecnai F30 field emission transmission electron microscope (TEM).

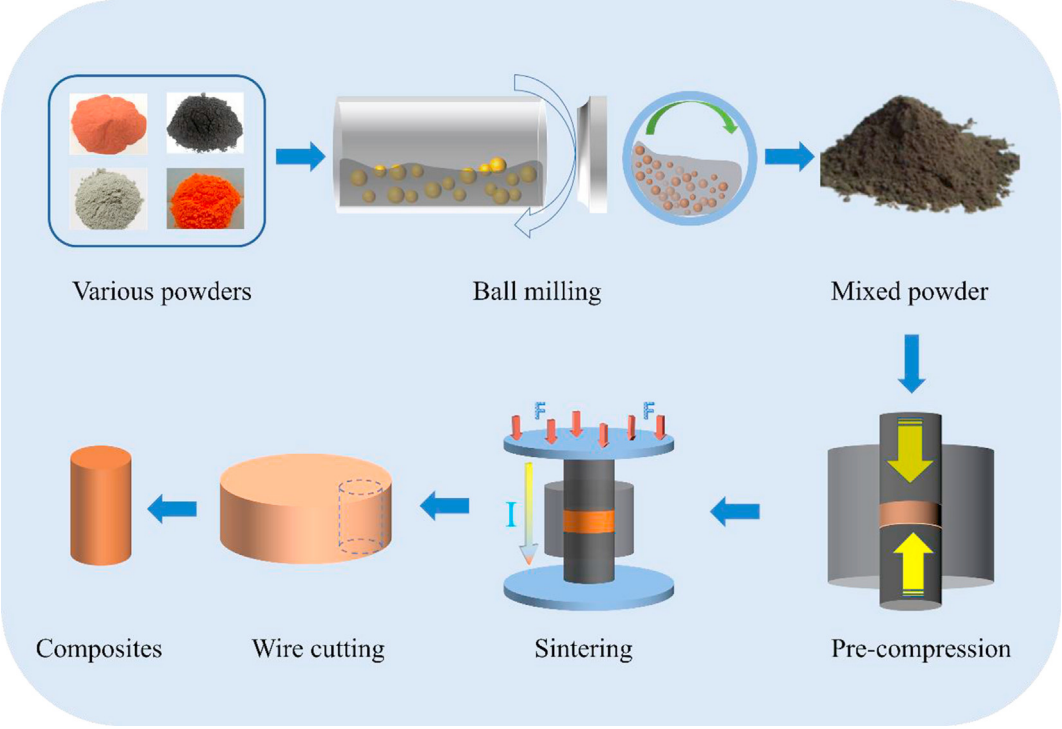

Fig. 2 – Schematic diagram of the composite preparation process.

2.3. Electrical contact experiments

Electrical contact is formed between two conductors and involves electrical current flow. Proper electrical contact performance is important in electrical appliances, power, automatic control, and information systems [48–50]. In order to test the electrical contacts, sintered samples were processed into Φ3.8 × 10 mm standard-size electrical contacts. The JF04C system was used to test the electrical contact behavior. Before the experiment, the surface of the electrical contacts was polished smooth with sandpaper to reduce the experimental error. An electronic balance with an accuracy of 0.1 mg was used to measure the mass of each contact sample before and after the test. Each contact was weighed 5 times and the mass was averaged. The mass difference before and after the test, Δm, was used to represent the material loss and transfer during the electrical contact process.

$$\Delta m = m_a - m_b \quad (1)$$

Here, m_b is the mass of electrical contacts before testing, and m_a is the mass of electrical contacts after testing. Four groups of samples were tested for each component. The test process was carried out in the constant current mode, the experimental voltage was 25 V, and the current was 10 A, 20 A, 25 A, and 30 A, respectively. Each group of samples was subjected to 5000 contact opening and closing cycles, in which the upper contact was the moving anode, and the lower contact was the static cathode. During the electrical contact, the contact force was 0.4–0.6 N. The arc erosion characteristics and three-dimensional morphology of the contact surface were observed after the test. The arc burning time and arc burning energy of the contact material during the opening and closing process were dynamically monitored. The experimental data were analyzed after the test.

3. Results and discussion

3.1. Material properties and microstructure

Table 1 lists the comprehensive properties of the Al_2O_3–Cu/30W3SiC and Al_2O_3–Cu/30W3SiC-0.5Y_2O_3 composites, including relative density, electrical conductivity, microhardness and thermal conductivity. The density of the samples prepared by the fast hot-pressing sintering was above 98%. After adding 0.5 wt% Y_2O_3, the density and conductivity of the material were slightly reduced, but the microhardness was improved. The electrical conductivity of the two materials was 58.3% IACS and 59.3% IACS, respectively, and the Vickers microhardness was 179 HV and 183 HV, respectively. Y_2O_3 particles can increase the diffusion barrier of the Cu matrix to a certain extent, delay the formation and growth of sintering necks, and inhibit the sintering of Cu [51]. On the one hand, Y_2O_3 has good thermal stability and poor electrical conductivity, so the addition of Y_2O_3 will hinder the continuity of the matrix interface and increase the scattering effect of free electrons, thereby reducing the conductivity of the material. On the other hand, Y_2O_3 hinders the growth of material grains, refines the grains, and acts as a secondary phase particle to hinder the movement of dislocations, which has a positive effect on the hardness. The thermal conductivity of Al_2O_3–Cu/30W3SiC and Al_2O_3–Cu/30W3SiC-0.5Y_2O_3 composites are 108 W/(m·k) and 275 W/(m·k), respectively, and the addition of Y_2O_3 increases the thermal conductivity of the materials by 154%. The thermal conductivity of the composite is substantially improved. It makes the material dissipate heat better and work more stably in the process of use.

Cu is easily oxidized in the air to form non-conductive oxides. During the work of the electrical contacts, once a large number of oxides are formed, the contact resistance of the electrical contact material rises and the material generates a lot of heat. The stability and reliability of the use of electrical contact materials have a certain impact. Using an electric thermostatic chamber furnace, the specimens were charged at a constant temperature of 150 °C for oxidation testing, and the oxidation time was 20 h. The surface of the specimen was polished smooth and washed with anhydrous ethanol to remove surface impurities before testing. Calculate the value of oxidation weight gain per unit surface area of materials.

$$\eta = (M_2 - M_1)/S \quad (2)$$

The formula η is the oxidation weight gain per unit surface area of the material; M_1 is the mass of the specimen before oxidation; M_2 is the mass of the specimen after oxidation; S is the surface area of the specimen.

After testing, the oxidation weight gain per unit surface area of Al_2O_3–Cu/30W3SiC and Al_2O_3–Cu/30W3SiC-0.5Y_2O_3 composites were 9.3 mg/cm^2 and 8.4 mg/cm^2, respectively. On the one hand, the composites have high density and dense structure. It is difficult for oxygen atoms to enter into the surface layer of the material along enough pores. W、SiC itself has a high antioxidant capacity, which can improve the antioxidant performance of the composites. On the other hand, Al_2O_3 and Y_2O_3 are diffusely distributed in the material matrix tissue, which have a pegging effect on composites matrix structure. It hinders the outward diffusion of metal ions, which makes the oxidation of composites mainly rely on the inward penetration of oxygen atoms. The oxidation rate of composites is reduced, thus improving the oxidation resistance of composites.

In order to explore the existing state of the elements of the two composite materials after sintering, XRD was used to analyze the phases of the sintered composites. As seen in

Table 1 – Comprehensive properties of composite materials.

Composite	Relative density, %	Electrical conductivity, % IACS	Vickers hardness, HV	Thermal conductivity, W/(mk)
Al_2O_3–Cu/30W3SiC	98.6	59.3	179	108
Al_2O_3–Cu/30W3SiC-0.5Y_2O_3	98.1	58.3	183	275

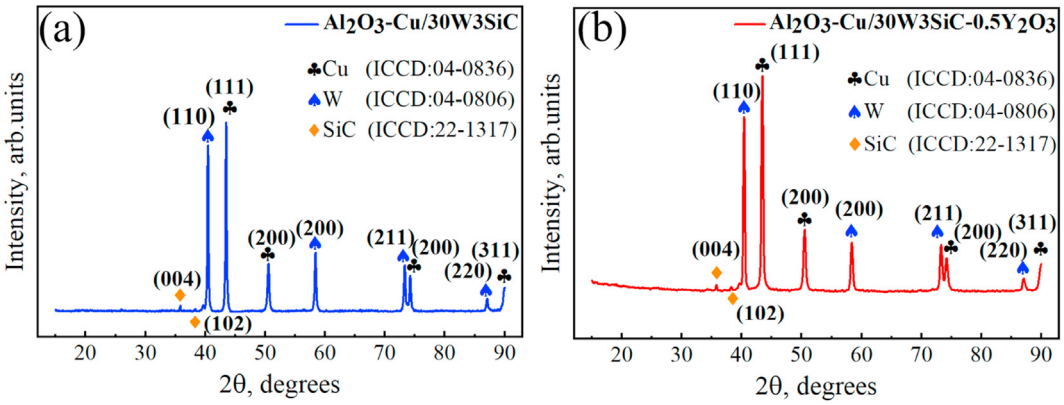

Fig. 3 – XRD patterns of the composites: (a) Al_2O_3–Cu/30W3SiC; (b) Al_2O_3–Cu/30W3SiC-0.5Y_2O_3.

Fig. 3, within the 15–90° diffraction angle range, XRD reflections corresponding to the Cu, W, and SiC strengthening phases were found. The XRD diffraction reflections at $2\theta = 40.7°$, 58.8°, 73.7°, and 97.6° correspond to the (110), (200), (211), and (220) crystal planes of W, while at $2\theta = 36.4°$ and 38.4° they correspond to the (004) and (102) crystal planes of SiC, respectively. The XRD phase analysis results of the two composite materials are practically the same. Due to the low content of Y_2O_3 and Al_2O_3, their characteristic reflections are not visible in the XRD energy spectra, and no other impurity reflections were found in the spectra.

In order to observe the sintering of powder and the microstructure of the sample, SEM images and EDS data of the sintered samples were analyzed. Fig. 4(a) and (c) are SEM images of the Al_2O_3–Cu/30W3SiC and Al_2O_3–Cu/30W3SiC-0.5Y_2O_3 composites, respectively, with white being the W phase and black being the SiC phase. Fig. 4(b), (e), (d), and (f) are the corresponding EDS layered images, respectively. The two electrical contacts have a dense structure and no obvious defects such as holes and powder agglomeration were found. W particles and SiC hard strengthening phase are distributed in the copper matrix and Al_2O_3 is generated.

After the material was mechanically and ionically thinned, the transmission electron microscopy analysis of the relevant thin regions was performed. Fig. 5 shows the transmission electron microscopy (TEM) and high resolution TEM (HRTEM) images of the Al_2O_3–Cu/30W3SiC-0.5Y_2O_3 composite. The movement of dislocations is the microscopic form of material deformation, and blocking the movement of dislocations is one of the most important ways to strengthen materials. As seen in Fig. 5(a), many Al_2O_3 nanoparticles are generated in the copper matrix by internal oxidation, pinning the grain and subgrain boundaries to inhibit the nucleation of dynamic recrystallization. The dislocation movement needs to bypass or cut through the Al_2O_3 secondary phase particles, which increases the resistance of the dislocation movement, thereby hindering the dislocation movement and causing the dislocation accumulation. The addition of Al_2O_3 particles plays a role in dispersion strengthening, inhibiting the movement of grain boundaries, thereby inhibiting the recrystallization and grain growth of the Cu matrix, and increasing the comprehensive mechanical properties of the material. Fig. 5(b) shows the diffraction spots corresponding to the copper matrix and the Al_2O_3 dispersed phase after the fast Fourier transformation (FFT), where the crystal band axes of Cu and Al_2O_3 are [01 $\bar{1}$] and [1 $\bar{1}$ 0], respectively. Fig. 5(c) shows the TEM image of W and SiC and the corresponding selected area electron diffraction (SAED) pattern, which determined the W

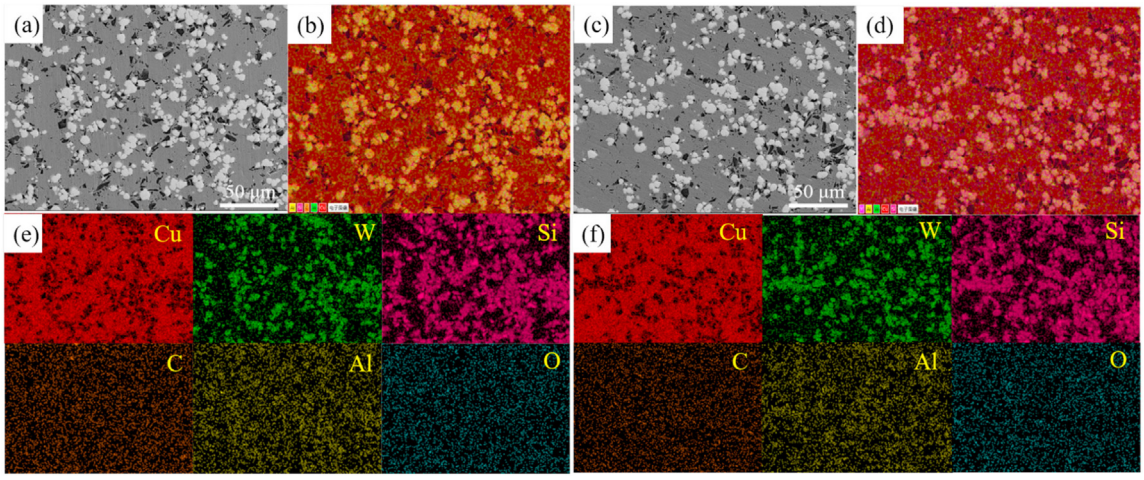

Fig. 4 – SEM images and EDS layered images of composite materials. (a, b, and e) Al_2O_3-Cu/30W3SiC; (c, d, and f) Al_2O_3-Cu/30W3SiC-0.5Y_2O_3.

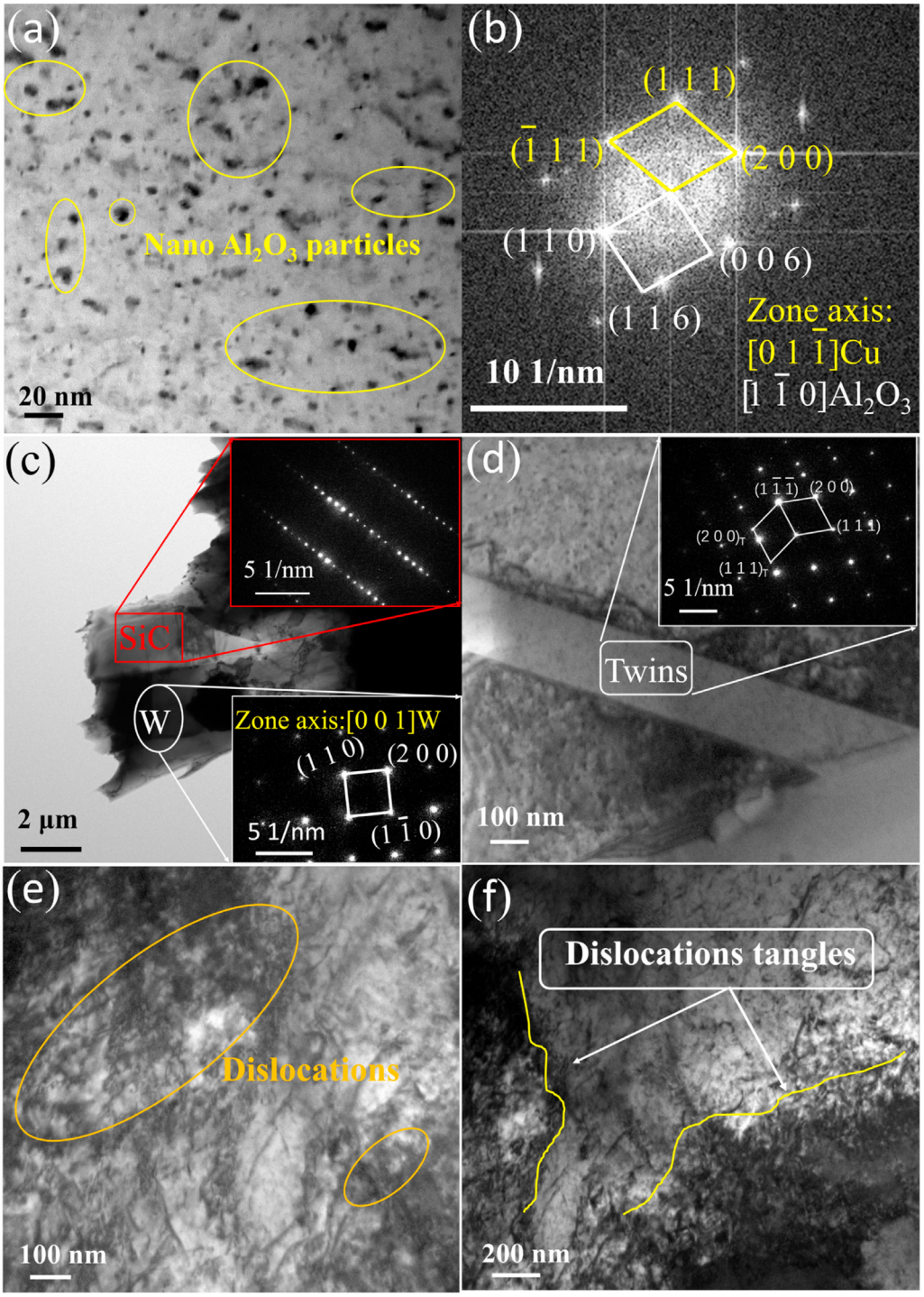

Fig. 5 – TEM and SAED images of the Al_2O_3–Cu/30W3SiC-0.5Y_2O_3 composite. (a) Morphology of nano Al_2O_3 particles, (b) FFT of Cu and Al_2O_3, (c) microstructure and SAED of W and SiC, (d) twins and their lattice parameters, (e, f) dislocation tangles.

phase by calibration, and the lattice parameters are a = b = c = 0.31648 nm, α = β = γ = 90°, [001] ribbon axis. W and Cu are immiscible with each other. With high hardness and good wear resistance, W is uniformly distributed in the Cu matrix as a strengthening phase, as W hinders the movement of dislocations, causing dislocation accumulation and increasing the hardness of the material. As a kind of hard ceramic particle with excellent properties, SiC can significantly improve the hardness and service life of materials. Twins are also present in Fig. 5(d), where the lattices on both sides of the twin boundaries are mirror-symmetrical, and the existence of twins has a positive effect on the strength and hardness of the material. The strengthening mechanism by twin boundaries effectively hinders dislocation movement,

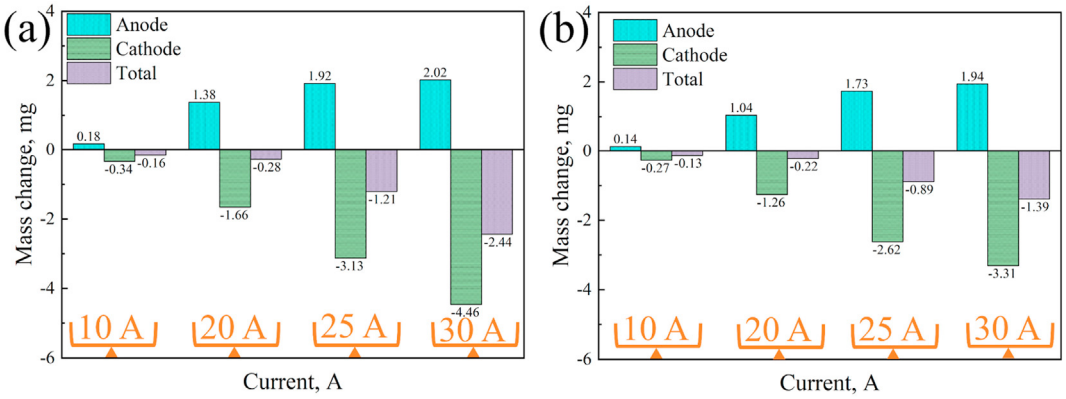

Fig. 6 – Cathode, anode, and total mass changes before and after the electrical contact experiments: (a) Al_2O_3–Cu/30W3SiC; (b) Al_2O_3–Cu/30W3SiC-0.5Y_2O_3.

thereby strengthening the material. Fig. 5(e) and (f) show the entangled dislocations in the copper matrix. Because of the various reinforcing phases in the material, the movement of dislocations is hindered, and dislocations are entangled with each other during the movement to form dislocation walls and cells. The greater the dislocation density, the stronger the ability of the metal to resist plastic deformation, which is the main way to enhance its performance.

3.2. *Electrical contact experiments and analysis*

During electrical contact, the arc erosion resistance of the contact material and the amount of material transfer and loss directly affect the service life of the components [52,53]. Fig. 6 shows the mass change of Al_2O_3–Cu/30W3SiC and Al_2O_3–Cu/30W3SiC-0.5Y_2O_3 electrical contact materials at 25 V DC under different current conditions of 10 A, 20 A, 25 A, and 30 A after 5000 opening-closing contact cycles. The mass change trend of the two materials is the same. At different currents, the mass of the anode material increases while the mass of the cathode decreases, which indicates the transfer of material from the cathode to the anode during the electrical contact. The total mass change is negative, indicating that some materials enter the surrounding environment, and as the current increases, the amount of material transfer and loss increases. The loss mechanism of the material was explored, and it was found that when the contact moved from the closed to the open position, the contact surface and conductive surface of the cathode and anode contacts decreased, and the corresponding contact resistance of the contacts increased. When contact is about to disconnect, the I^2R energy is concentrated at an extremely small area, which will rapidly increase the contact temperature above the melting point of the metal, causing metal bumping and explosive gasification. When the cathode and anode are filled with metal vapor, an arc will be formed, and the contact material will evaporate and splash. The positive ions in the arc column bombard the arc root area of the cathode at high speed. The contact gap can be relatively long, several times the average free travel of the gap electrons. The collision of electrons between the arc columns causes energy loss before reaching the anode, and the energy is greatly reduced after reaching the anode. The positive ions between the arc columns are accelerated by the electric field and electrons and bombard the surface of the cathode contact at a high speed. The cathode material evaporates more than the anode, and the material is transferred from the cathode to the anode and partially to the surrounding environment, resulting in material transfer and mass loss [54]. At the moment before the cathode and anode contacts are disconnected, the energy of the liquid bridge of the metal arc column is:

$$Q = \int_0^{t_L} U_L(t) i_L(t) dt \tag{3}$$

Here, t_L is the duration of the liquid bridge current before the contact is disconnected, $U_L(t)$ is the voltage across the liquid bridge before the contact is disconnected, and $i_L(t)$ is the current through the liquid bridge before the contact is disconnected.

Adding W with a high melting point and low saturated vapor pressure to the Cu matrix will increase the melting point of the material. When the temperature of the contact increases sharply during the electrical contact process, the W particles deform to form a needle-like W skeleton [1], which restricts the fluidity of the melt, thereby increasing the arc erosion resistance of the material and reducing the mass transfer and loss of the material. Fig. 6 shows the mass changes of the cathode and anode and the total mass of the two materials before and after the electrical contact experiment at different currents. It can be seen from Fig. 6 that when the 0.5 wt% Y_2O_3 were added, the mass transfer and loss of the material were reduced. This is because the high temperature generated by the arc during the breaking process of the contacts will partially melt the surface of the electrical contacts. Y_2O_3 has good high-temperature stability and copper melt wettability, which can reduce the splash of copper melt, reduce the mass transfer of cathode and anode, and the loss of material to the surrounding environment, thereby improving its arc resistance. The addition of nano Y_2O_3 can enhance the material through the dispersion strengthening mechanism, but due to the poor conductivity of Y_2O_3 and the scattering effect on free electrons, it has a certain impact on the conductivity of the material. In this experiment, the amount of

Y_2O_3 added is less, which has little effect on the electrical conductivity.

Fig. 7 shows the low-magnification morphology and corresponding three-dimensional topography of the cathode and anode contacts of the two composite materials after being opened and closed 5000 times at 25 V DC and 30 A. There are many protrusions on the surface of the anode contact, and there are many pits on the cathode contact. It can also be seen from the three-dimensional topography that when 0.5 wt% Y_2O_3 is added, the degree of anode protrusion and cathode depression of the contacts is reduced. All these indicate that the addition of Y_2O_3 improves the arc erosion resistance of the material.

Fig. 8 is a high-magnification scan of the surface of the cathode and anode contacts after being opened and closed 5000 times at 25 V DC and 30 A. At high magnification, the arc

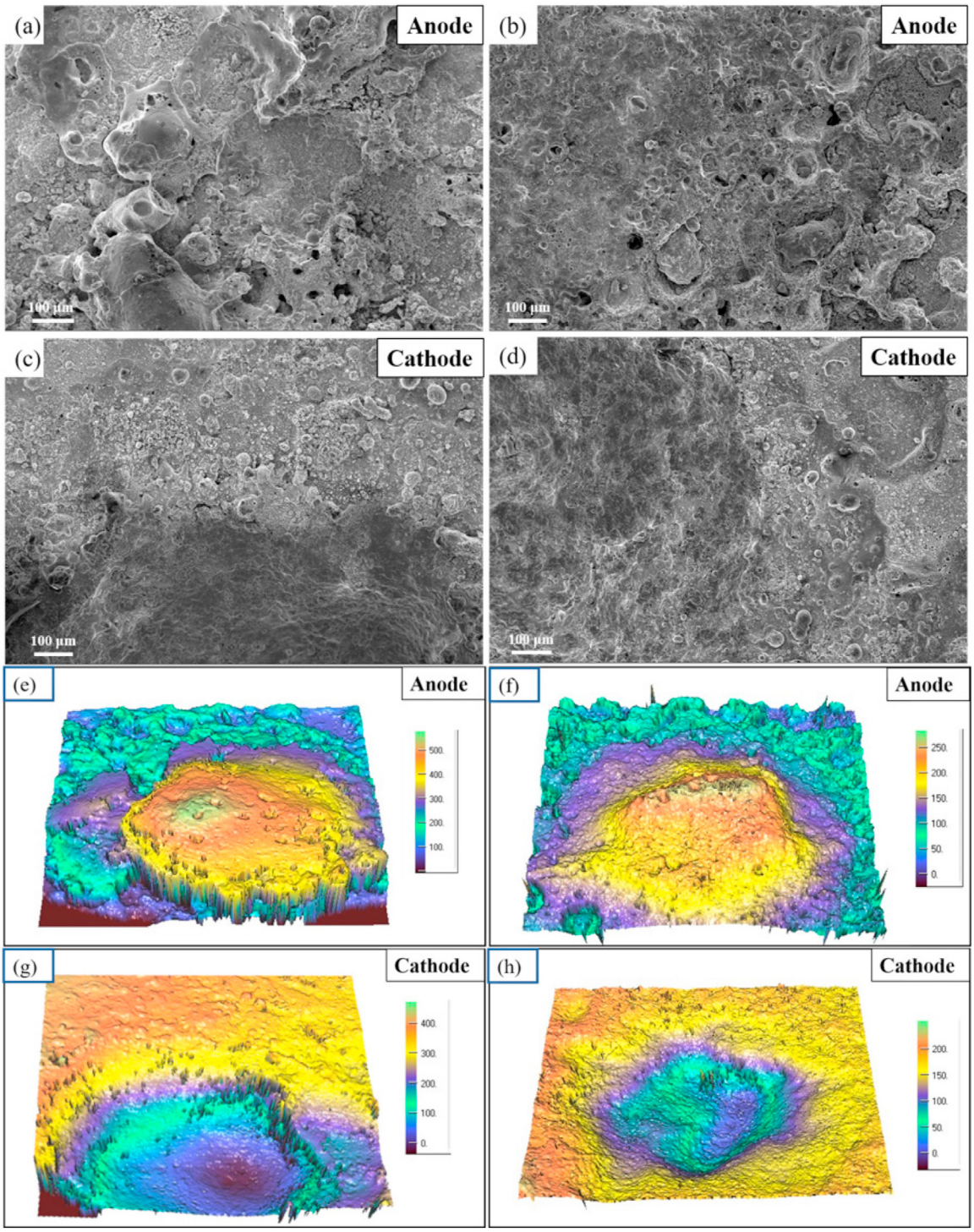

Fig. 7 – SEM images and corresponding 3D profiles of the arc erosion morphology on the contact surface (a, c, e, and g) Al_2O_3–Cu/30W3SiC; (b, d, f, and h) Al_2O_3–Cu/30W3SiC-0.5Y_2O_3.

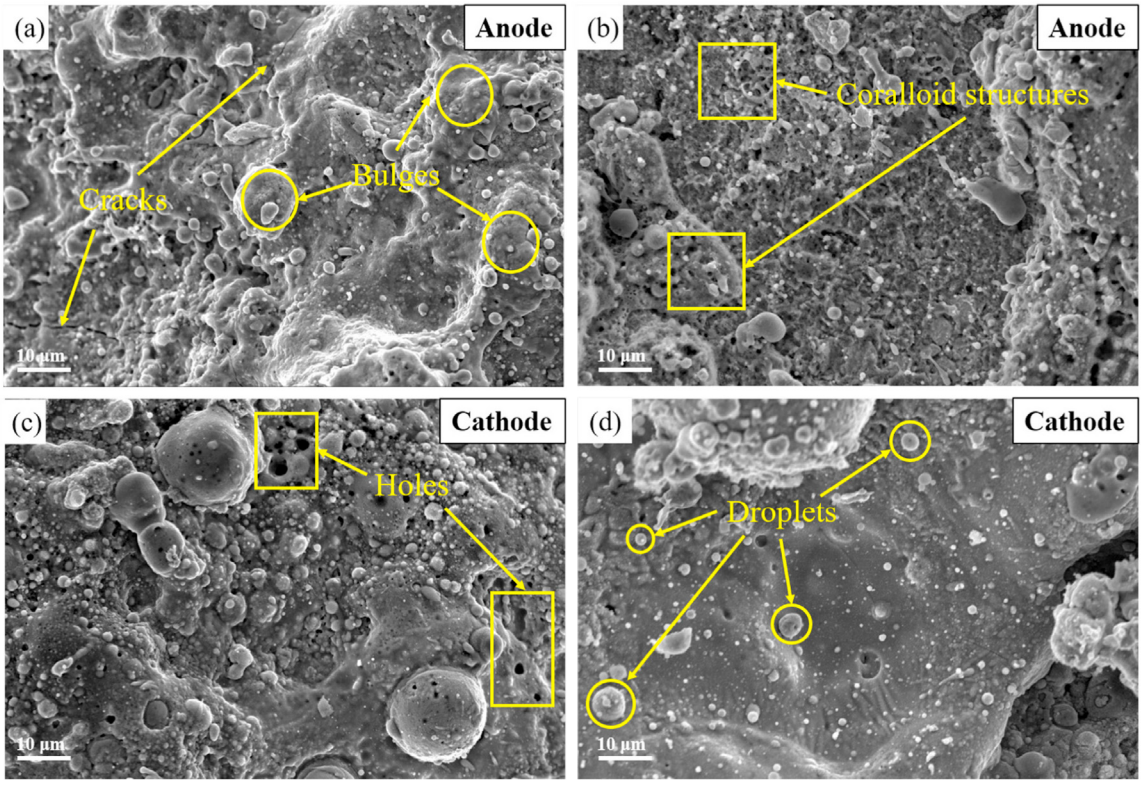

Fig. 8 – Typical morphological characteristics of electrical contact surface (a, b) anode; (c, d) cathode.

erosion morphology and some typical features of the material can be seen, such as bulges, depressions, holes, droplets, cracks, and coralloid structures formed by arc ablation. Since the material is transferred from the cathode to the anode, the protrusions mainly appear on the surface of the anode contacts, and the depressions mainly appear on the surface of the cathode contacts. When the material is in contact, the arc between the contacts causes the thermal effect to increase the temperature of the arc column area, and the material in this area undergoes bumping and splashing. However, the temperature in the area outside the arc column is far lower than in the arc center. When the molten and splashed liquid metal enters the lower temperature area, the cooling rate of the material is extremely fast, and the liquid metal on the contact surface has solidified before it can be spread out. The larger molten metal will form a coral-like structure, and the smaller molten metal will solidify to form droplets, as seen in Fig. 8(b) and (d). Due to the fast cooling rate and thermal stress gradient of the molten layer on the surface of the contact, holes and cracks will be generated on the contact surface, which are common morphological features on all contact surfaces. The existence of holes and cracks has a negative impact on the arc erosion resistance of the contacts. The existence of holes will reduce the mechanical strength of the molten layer of the contacts, thereby causing cracks. Cracks are dangerous morphological features on the surface of electrical contacts. Once the cracks extend, the material on the surface of the contacts may fall off, accelerating the failure of the contacts. The addition of Y_2O_3 improves the wettability of the copper matrix, which inhibits the generation of these undesirable topographical features and increases the service life of the contacts.

In the process of electrical contact, when the current and voltage reach a certain value, the fuse link is just melted and disconnected, and an arc will be formed between the two contacts. Due to the Joule heating, the center temperature of the arc is very high, which leads to erosion of the contact surface and accelerated failure. Therefore, it is particularly important to improve the arc-extinguishing ability of the electrical contact material. The arc-starting and arc-extinguishing ability of the material can be illustrated by the arc duration during electrical contact. The longer the arc duration, the more arc erosion the material will experience and the earlier the contacts will fail. Fig. 9 shows the change of arc duration during 5000 cycles of opening and closing contact at 25 V DC and 10 A, 20 A, 25 A, and 30 A for two materials. Each time the contacts are opened and closed 100 times an average is taken. In general, the arc duration of the two materials is kept at a low level. With the increase of the current, the arc duration increases, and the arc erosion is more serious. W has a high melting point, good thermal conductivity, and high heat capacity. The addition of W to copper-based electrical contact materials reduces the hot electron emission and metal vapor in the arc. This inhibits material dissociation and increases arc resistance, allowing for faster arc initiation and breaking of electrical contacts. Fig. 9(d) shows the average arc duration of the electrical contacts of the two materials during the electrical contact process. The average arc duration of the electrical contacts with the Al_2O_3–Cu/30W3SiC composition is 4.48 ms, 5.72 ms,

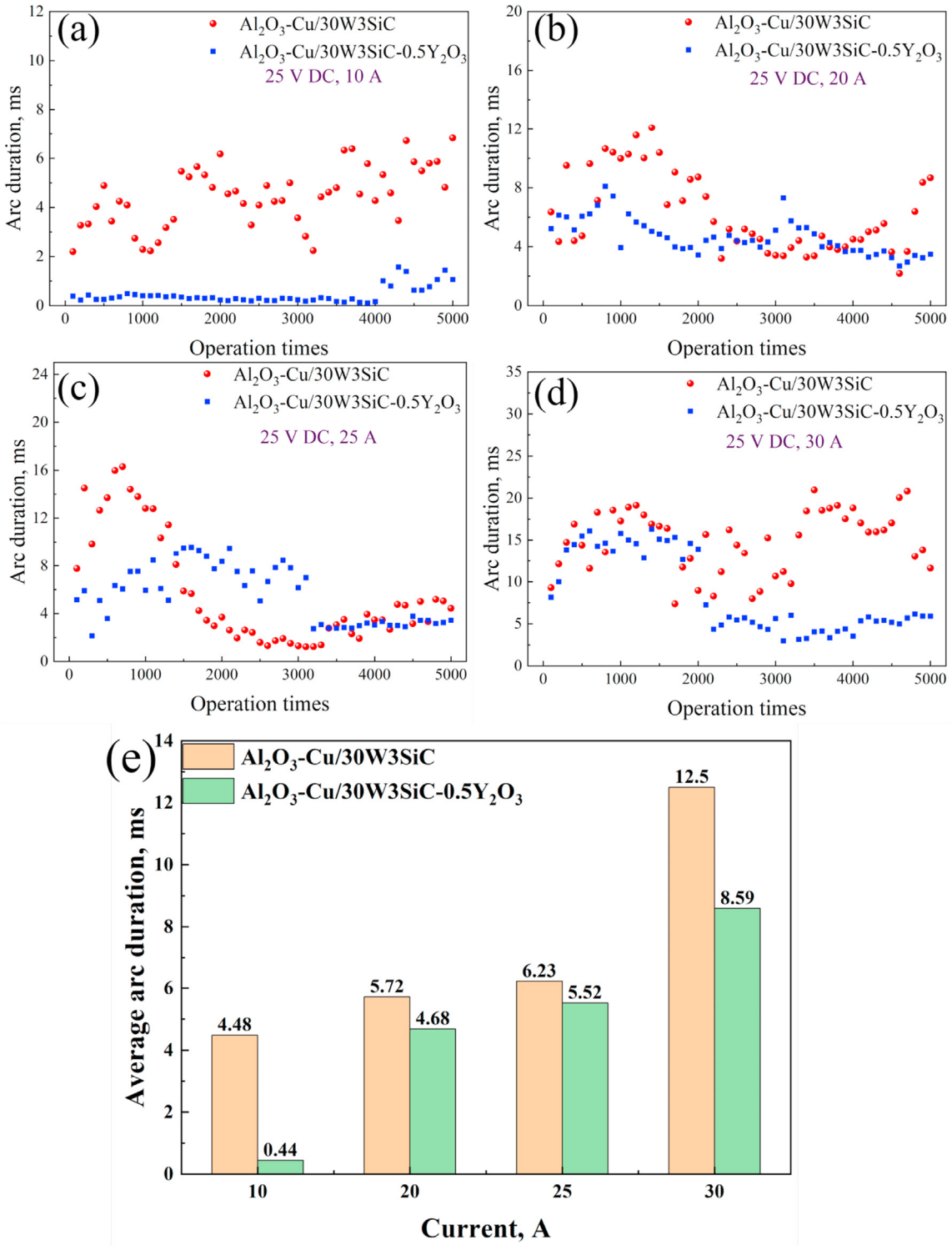

Fig. 9 – Variation of arc duration of materials during electrical contact:(a) 10 A; (b) 20 A; (c) 25 A; (d) 30 A; (e) Average arc duration.

6.23 ms, and 12.5 ms, respectively. The average arc duration of the electrical contacts with the Al_2O_3–Cu/30W3SiC-0.5Y_2O_3 composition is 0.44 ms, 4.68 ms, 5.52 ms, and 8.59 ms, respectively. In comparison, after adding Y_2O_3, the arc duration of the material is greatly reduced, and the resistance to arc erosion is enhanced.

Fusion welding between contacts is one of the main forms of switch failure. During the process of opening or closing the circuit, the liquid metal bridge is generated between the contacts due to the pre-breakdown arc during closing or the arc formed during the bouncing of contacts or fusion welding due to arc heat flow melting the contact surface [52,55]. When

the switch is opened and closed, the force that must be applied to separate the moving and static contacts becomes the welding force of the material. The magnitude of the welding force can be used to evaluate the welding phenomenon of the material. Fig. 10 shows the change of the welding force of the two materials in electrical contact and the welding force of the material increases with the current. However, the welding force of the two materials is at a low level, not exceeding 0.5 N, and the welding force is significantly reduced after the addition of Y_2O_3. Under the experimental conditions of different currents of 10 A, 20 A, 25 A, and 30 A, the material fusion welding force after adding Y_2O_3 was 58.9%, 81.4%, 87.5%, and 89.4% of that without Y_2O_3, respectively. On the one hand, the internal oxidation disperses Al_2O_3 particles in the copper matrix. Adding a high melting point W with high thermal conductivity and heat capacity, and low chemical

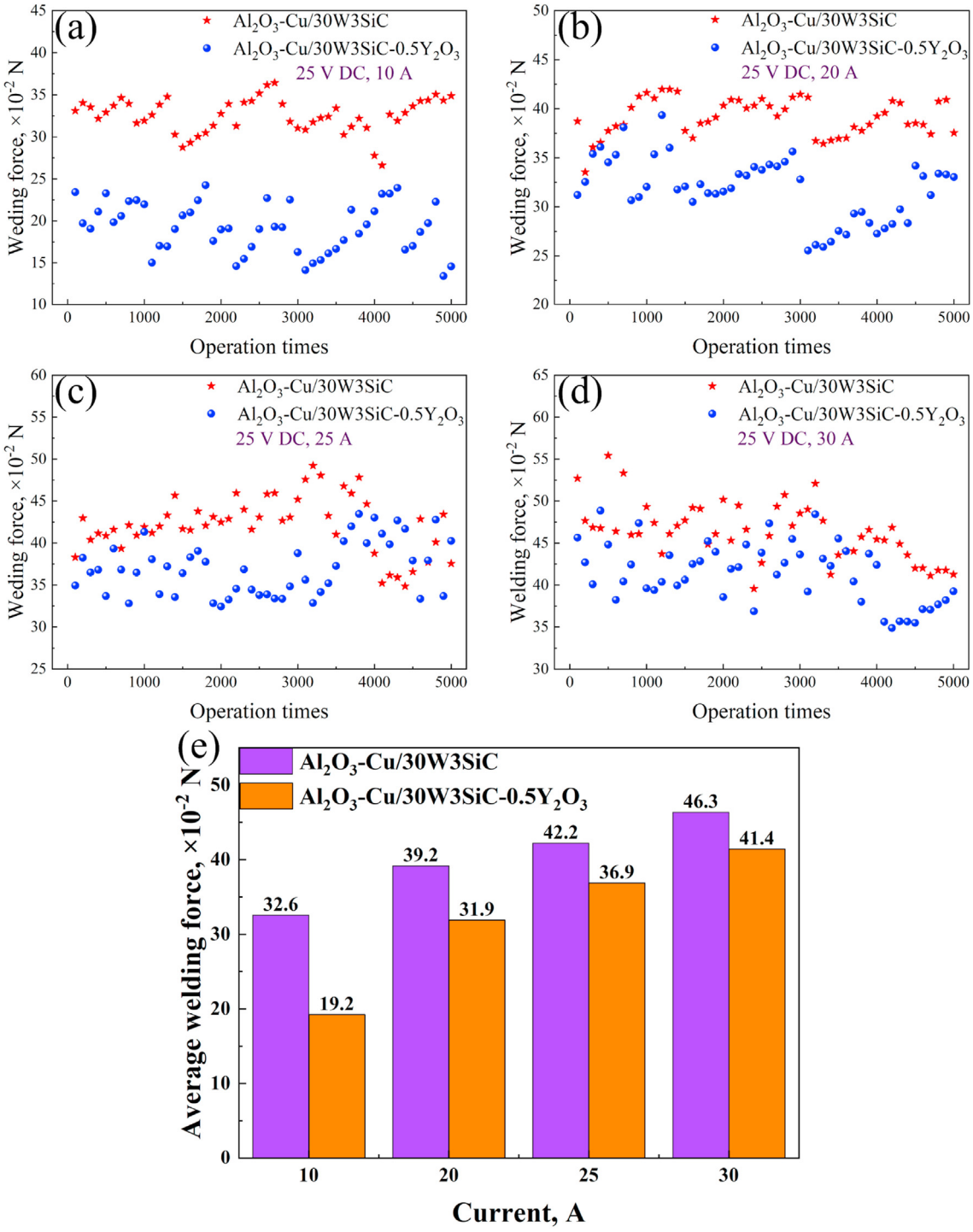

Fig. 10 – Variation of welding force of materials during electrical contact:(a) 10 A; (b) 20 A; (c) 25 A; (d) 30 A; (e) Average welding force.

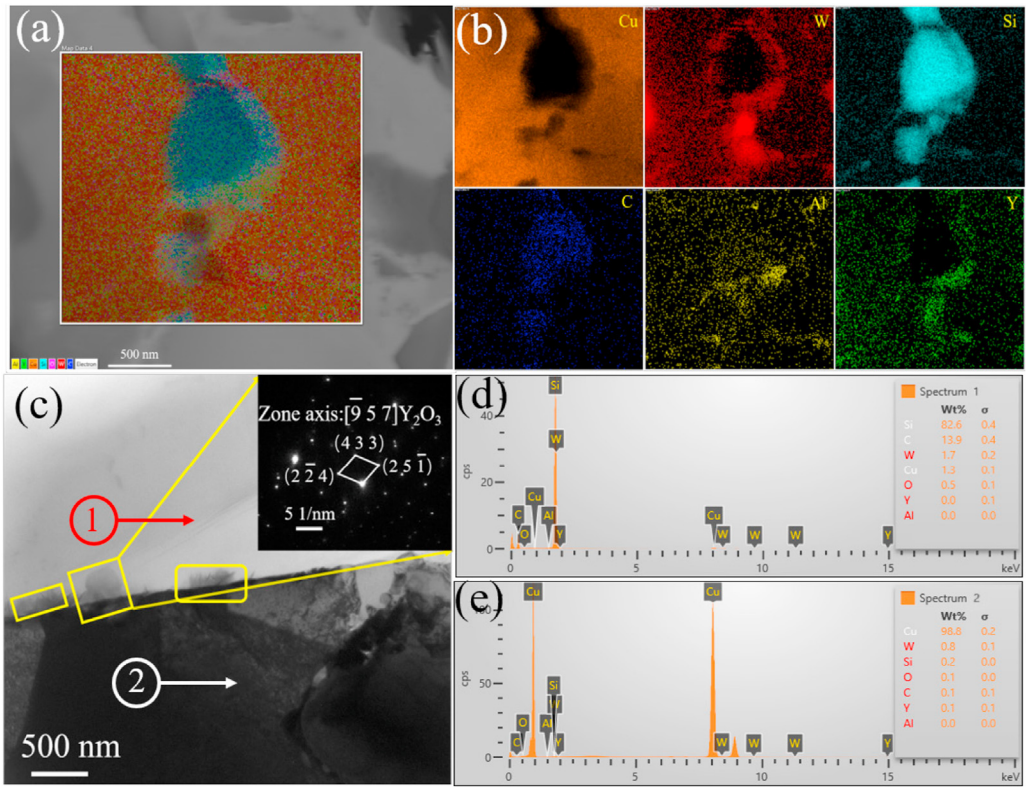

Fig. 11 – TEM micromorphology, SAED, and EDS analysis of the Al_2O_3–Cu/30W3SiC-0.5 Y_2O_3 composites: (a) EDS analysis; (b) element distribution of (a); (c) micromorphology and SAED of Y_2O_3; (d) EDS analysis of area 1; (e) EDS analysis of area 2.

affinity with Cu to form a Cu–W pseudo-alloy can weaken the welding force. On the other hand, Y_2O_3 improves the wettability of the copper melt and reduces the welding force of the material.

Adding 0.5 wt% Y_2O_3 to the Al_2O_3–Cu/30W3SiC resulted in a significantly enhanced arc erosion resistance of the material with an obvious strengthening effect. Fig. 11 shows the TEM microstructure along with SAED and EDS analysis of the Al_2O_3–Cu/30W3SiC-0.5Y_2O_3 composite. Fig. 11(a) shows the qualitative and quantitative analysis of the elemental composition of the selected area obtained by SEM and EDS. Fig. 11(b) is the surface element distribution diagram. Both Al_2O_3 and Y_2O_3 are dispersed in the Cu matrix, and Y_2O_3 is found in Cu, W, SiC, and other strengthening phases. Fig. 11(c) is the SEM image and the corresponding SAED analysis of the material, and (d) (e) are the EDS analysis results corresponding to the two positions 1 and 2 in (c), respectively. After calibration, it is found that there is the Y_2O_3 phase with a crystal band axis of [$\bar{9}$ 57] at the interface of Cu and SiC, and the lattice parameters are $a = b = c = 1.06041$ nm, $\alpha = \beta = \gamma = 90°$. Y_2O_3 is mainly at the interface because the addition of Y_2O_3 will cause lattice distortion, which will increase the system energy. In order to minimize the free energy, Y_2O_3 is distributed at the boundary, and evenly dispersed Y_2O_3 will also hinder the growth of copper grains and refine the grains. While increasing the mechanical properties of the material, the refinement of the grains also makes the Y_2O_3 more uniformly distributed at the Cu boundary. Y_2O_3 has good thermodynamic stability and fluorite-like structure, coupled with its unique copper melt wettability, which can significantly improve the arc erosion resistance of electrical contacts.

Based on combined material structure characterization, properties testing, material mass transfer during electrical contact, arc erosion profile, arc burning time, welding force, and many other experimental parameters, both Al_2O_3–Cu/30W3SiC and Al_2O_3–Cu/30W3SiC-0.5Y_2O_3 electrical contact materials have good performance. The nano Al_2O_3 generated by internal oxidation contributes greatly to the strengthening effects of the material, especially when Y_2O_3 is added, the material performs well during electrical contact, and the material properties remain good and stable after 5000 contact experiments, and there is a significant increase in the melt welding resistance and arc erosion resistance of the material. This work combines the previous work to develop copper matrix composites with excellent performance, which provides a new idea for the development of electrical contact materials and has important reference value.

4. Conclusions

1. Two kinds of electrical contact materials, Al_2O_3–Cu/30W3SiC and Al_2O_3–Cu/30W3SiC-0.5Y_2O_3, were prepared by the fast hot-pressing sintering technology and internal oxidation method. The density of the two kinds of composites are over 98%, the electrical conductivity is 58.3% IACS and 59.3% IACS, and the microhardness is 179 HV and 183 HV, respectively. Thermal conductivity is 108 W/(m·k) and 275 W/

(m·k), respectively. The structure of the two electrical contact materials is dense, and no obvious defects such as holes and powder agglomeration are found.

2. The microstructure of Al_2O_3–Cu/30W3SiC-0.5 Y_2O_3 was characterized, and a large number of Al_2O_3 nanoparticles was dispersed in the copper matrix, which hindered the movement of dislocations. In addition, it was also found that the comprehensive properties of the matrix were further enhanced by the uniformly dispersed W, SiC, and Y_2O_3, which hinder the dislocation movement inside the material.

3. The electrical contact experiment was carried out on the electrical contacts composed of Al_2O_3–Cu/30W3SiC and Al_2O_3–Cu/30W3SiC-0.5Y_2O_3. Y_2O_3 has good thermodynamic stability and wettability. Adding 0.5 wt% Y_2O_3 significantly reduced the mass transfer and loss of the contact material during the electrical contact process, and the arc duration and welding force were also significantly reduced, which indicates that Y_2O_3 improves the arc erosion resistance.

Author contribution

Xianhua Zheng: Investigation, Experiment, Formal analysis, Writing - review & editing. **Meng Zhou:** Resources, Theoretical analysis, Formal analysis. **Yi Zhang:** Formal analysis, Writing– review & editing. **JinLiang Huang:** Writing - review & Supervision. **Yunzhang Li:** Experiment, Formal analysis. **Hanjing Zhu:** Data curation, Formal analysis. **Shunlong Tang:** Investigation. **De Li:** Data curation, Formal analysis. **Shengli Liang:** Data curation, Formal analysis. **Baohong Tian:** Theoretical analysis, Supervision. **Yong Liu:** Visualization. **Xu Li:** Investigation, Formal analysis. **Yanlin Jia:** Formal analysis. **Alex A. Volinsky:** Writing - review & editing.

Declaration of competing interest

The authors declare that they have no known competing financial interests or personal relationships that could have appeared to influence the work reported in this paper.

Acknowledgments

This research was supported by the National Natural Science Foundation of China (52071134), the Program for Innovative Research Team at the University of Henan Province (22IRTSTHN001), China Postdoctoral Science Foundation (2020M682316, 2021T140779), Scientific Research and Development Special Project of the Henan Academy of Sciences (220910009), Key R&D and Promotion Projects in the Henan Province (212102210117).

REFERENCE

[1] Li HY, Wang XH, Hu ZD, Liu YF. Investigation of arc erosion mechanism for tin dioxide-reinforced silver-based electrical contact material under direct current. J Electron Mater 2020;49:4730–40. https://doi.org/10.1007/s11664-020-08193-9.

[2] Mousavi Z, Pourabdoli M. Physical and chemical properties of Ag–Cu composite electrical contacts prepared by cold-press and sintering of silver-coated copper powder. Mater Chem Phys 2022;290:126608. https://doi.org/10.1016/j.matchemphys.2022.126608.

[3] Varol T, Canakci A. The effect of flake microstructure on the preparation and properties of Cu-graphite sintered nanocomposites. Powder Metall Met Ceram 2016;55:426–36. https://doi.org/10.1007/s11106-016-9823-y.

[4] Güler O, Varol T, Alver Ü, Biyik S. The wear and arc erosion behavior of novel copper based functionally graded electrical contact materials fabricated by hot pressing assisted electroless plating. Adv Powder Technol 2021;32(8):2873–90. https://doi.org/10.1016/j.apt.2021.05.053.

[5] Yuan JH, Gong LK, Zhang WQ, Zhang B, Wei HG, Xiao XP, et al. Work softening behavior of Cu–Cr–Ti–Si alloy during cold deformation. J Mater Res Technol 2019;8:1964–70. https://doi.org/10.1016/j.jmrt.2019.01.012.

[6] Varol T, Canakci A. The effect of type and ratio of reinforcement on the synthesis and characterization Cu-based nanocomposites by flake powder metallurgy. J Alloys Compd 2015;649:1066–74. https://doi.org/10.1016/j.jallcom.2015.07.008.

[7] Varol T, Canakci A. Microstructure, electrical conductivity and hardness of multilayer graphene/Copper nanocomposites synthesized by flake powder metallurgy. Met Mater Int 2015;21:704–12. https://doi.org/10.1007/s12540-015-5058-6.

[8] Torresani E, Carrillo M, Haines C, Martin D, Olevsky E. Fabrication of powder components with internal channels by spark plasma sintering and additive manufacturing. J Eur Ceram Soc 2022;43(3):1117–26. https://doi.org/10.1016/j.jeurceramsoc.2022.11.008.

[9] Novák P, Benediktová D, Mestek S, Tsepeleva A, Kopeček J. Aluminum alloys with natural ratio of alloying elements manufactured by powder metallurgy. J Alloys Compd 2022;931:167440. https://doi.org/10.1016/j.jallcom.2022.167440.

[10] Zhumadilov R, Slamyiya M, Dosbolayev M, Ramazanov T. Obtaining of composite metal-carbon nanoparticles by magnetron sputtering. Mater Today Proc 2020;31(2):464–8. https://doi.org/10.1016/j.matpr.2020.06.014.

[11] Rajput R, Raut A, Setti SG. Prediction of mechanical properties of aluminium metal matrix hybrid composites synthesized using Stir casting process by Machine learning. Mater Today Proc 2022;59(3):1735–42. https://doi.org/10.1016/j.matpr.2022.04.316.

[12] Majzoobi GH, Jafari SS, Rahmani K. A study on damage evolution in Cu–TiO_2 composite fabricated using powder metallurgy followed by hot extrusion. Mater Chem Phys 2022;290:126140. https://doi.org/10.1016/j.matchemphys.2022.126140.

[13] Alessandro S, Raja H, Khan U, Sandeep I, Martina M, Advenit M, et al. Development of Ni-base metal matrix composites by powder metallurgy hot isostatic pressing for space applications. Adv Powder Technol 2022;33(2):103411. https://doi.org/10.1016/j.apt.2021.103411.

[14] Abhishek P, Vimal E, Abhishek BM, Chandra SP, Rajneesh H, Satish VK. In-situ interfacial growth of TiAl intermetallic and its influence on microparticle dislodgement during abrasive wear of Al/Ti6Al4V composite. Mater Today Commun 2020;24:101123. https://doi.org/10.1016/j.mtcomm.2020.101123.

[15] Varol T, Canakci A. An investigation on wear behavior of Cu-graphite nanocomposites prepared by flake powder

metallurgy. Ind Lubric Tribol 2017;69:8–14. https://doi.org/10.1108/ILT-11-2015-0187.
[16] Kasagi T, Yamamoto S. Effect of particle shape on electrical conductivity and negative permittivity spectra of Cu granular composite materials. J Mater Sci Mater Electron 2021;22:4974–83. https://doi.org/10.1007/s10854-021-07686-5.
[17] Yang M, Hu YL, Li XN, Li ZM, Zheng YH, Li NJ, et al. Compositional interpretation of high elasticity Cu-Ni-Sn alloys using cluster-plus-glue-atom model. J Mater Res Technol 2022;17:1246–58. https://doi.org/10.1016/j.jmrt.2022.01.075.
[18] Shayan M, Eghbali B, Niroumand B. Fabrication of AA2024–TiO_2 nanocomposites through stir casting process. Science Direct 2020;30(11):2891–903. https://doi.org/10.1016/S1003-6326(20)65429-2.
[19] Su H, Gao WL, Feng ZH, Lu Z. Processing, microstructure and tensile properties of nano-sized Al_2O_3 particle reinforced aluminum matrix composites. Mater Des 2012;36:590–6. https://doi.org/10.1016/j.matdes.2011.11.064.
[20] Abaker Z, Hussein T, Makawi S, Mustafa B, Modwi A. Superior uptake of Cu(II) from aquatic media via Y_2O_3-ZnO nanostructures. Nano-Struct & Nano-Objects 2022;30:100879. https://doi.org/10.1016/j.nanoso.2022.100879.
[21] Güler O, Varol T, Alver Ü, Canakci A. Effect of Al_2O_3 content and milling time on the properties of silver coated Cu matrix composites fabricated by electroless plating and hot pressing. Mater Today Commun 2020;24:101153. https://doi.org/10.1016/j.mtcomm.2020.101153.
[22] Tian BH, Liu P, Song KX, Li Y, Liu Y, Ren FZ, Su JH. Microstructure and properties at elevated temperature of a nano-Al_2O_3 particles dispersion-strengthened copper base composite. Mater Sci Eng, A 2012;435–436:705–10. https://doi.org/10.1016/j.msea.2006.07.129.
[23] Zhou HO, Tang JC, Ye N. A novel approach for strengthening Cu–Y_2O_3 composites by in situ reaction at liquidus temperature. Mater Sci Eng, A 2013;584:1–6. https://doi.org/10.1016/j.msea.2013.07.007.
[24] Zhang XH, Zhang Y, Tian BH, An JC, Zhao Z, Volinsky AA. Arc erosion behavior of the Al_2O_3-Cu/(W, Cr) electrical contacts. Compos B Eng 2019;160:110–8. https://doi.org/10.1016/j.compositesb.2018.10.040.
[25] Mu Z, Geng HR, Li MM, Nie GL, Leng JF. Effects of Y_2O_3 on the property of copper based contact materials. Compos B Eng 2013;52:51–5. https://doi.org/10.1016/j.compositesb.2013.02.036.
[26] Li WS, Dong HF. Effect of nano-Y_2O_3 on microstructure and mechanical properties of W–Ni–Cu alloys. Mater Res Express 2018;5(10):106503. https://doi.org/10.1088/2053-1591/aad996.
[27] Satishkumar P, Mahesh G, Meenakshi R, Vijayan SNR. Tribological characteristics of powder metallurgy processed Cu- WC/SiC metal matrix composites. Mater Today Proc 2021;37(2):459–65. https://doi.org/10.1016/j.matpr.2020.05.449.
[28] Lu SL, Xiao P, Yuan D, Hu K, Wu SS. Preparation of Al matrix nanocomposites by diluting the composite granules containing nano-SiCp under ultrasonic vibration. J Mater Sci Technol 2018;34:1609–17. https://doi.org/10.1016/j.jmst.2018.01.003.
[29] Akborpour MR, Alipour S, Safarzadeh A, Kim HS. Wear and friction behavior of self-lubricating hybrid Cu-(SiC + x CNT) composites. Compos B Eng 2019;158:92–101. https://doi.org/10.1016/j.compositesb.2018.09.039.
[30] Câmara NT, Raimundo RA, Lourenço CS, Morais LM, Silva DS, Gomes RM, et al. Impact of the SiC addition on the morphological, structural and mechanical properties of Cu-SiC composite powders prepared by high energy milling. Adv Powder Technol 2021;32(8):2950–61. https://doi.org/10.1016/j.apt.2021.06.006.
[31] Raimundo RA, Costa FA, Morales MA, Silva AG, Gomes UU. Effect of the high energy milling on the microstructure of Cu-20%WC composite powders prepared with recycled WC. Int J Refract Metals Hard Mater 2020;90:105223. https://doi.org/10.1016/j.ijrmhm.2020.105223.
[32] Akbarpour MR, Mirabad HM, Alipour S. Microstructural and mechanical characteristics of hybrid SiC/Cu composites with nano- and micro-sized SiC particles. Ceram Int 2019;3(45):3276–83. https://doi.org/10.1016/j.ceramint.2018.10.235.
[33] Zhang YL, Li WB, Hu M, Yi HY, Zhou W, Ding PL, et al. Fabrication of SiC@Cu/Cu composites with the addition of SiC@Cu powder by magnetron sputtering. Int J Photoenergy 2021:6623776. https://doi.org/10.1155/2021/6623776.
[34] Palma RH, Sepulveda AO. Creep behavior of two Cu-2 vol% TiC alloys obtained by reaction milling and extrusion. Mater Sci Eng, A 2013;588:82–5. https://doi.org/10.1016/j.msea.2013.09.024.
[35] Li JY, Lu SL, Wu SS, Zhao DJ, Li F, Guo W. Effects of nanoparticles on the solution treatment and mechanical properties of nano-SiCp/Al-Cu composites. J Mater Process Technol 2021;296:117195. https://doi.org/10.1016/j.jmatprotec.2021.117195.
[36] Deshpande PK, Li JH, Lin RY. Infrared processed Cu composites reinforced with WC particles. Mater Sci Eng, A 2006;429:58–65. https://doi.org/10.1016/j.msea.2006.04.124.
[37] Zhao P, Guo SB, Liu GH, Chen YX, Li JT. Fabrication of Cu-riched W–Cu composites by combustion synthesis and melt-infiltration in ultrahigh-gravity field. J Nucl Mater 2013;441(1–3):343–7. https://doi.org/10.1016/j.jnucmat.2013.06.011.
[38] Shahidi ZK, Faraji G. Fabrication of W-Cu composite by wire crumpling and subsequent melt infiltration. Mater Lett 2022;321:132432. https://doi.org/10.1016/j.matlet.2022.132432.
[39] Zhang LM, Chen WS, Luo GQ, Chen PG, Shen Q, Wang CB. Low-temperature densification and excellent thermal properties of W–Cu thermal-management composites prepared from copper-coated tungsten powders. J Alloys Compd 2014;588:49–52. https://doi.org/10.1016/j.jallcom.2013.11.003.
[40] Fan JL, Liu T, Zhu S, Han Y. Synthesis of ultrafine/nanocrystalline W–(30–50)Cu composite powders and microstructure characteristics of the sintered alloys. Int J Refract Metals Hard Mater 2013;30(1):33–7. https://doi.org/10.1016/j.ijrmhm.2011.06.011.
[41] Amalu NI, Okorie BA, Ugwuoke JC, Obayi CS. Electrical conductivity of spark plasma sintered W-Cu and Mo-Cu composites for electrical contact applications. J Miner Mater Char Eng 2021;9:48–60. https://doi.org/10.4236/jmmce.2021.91004.
[42] Zhou LC, Zhang JL, Zhang QQ, Wang HL, Zhao Z, Chen QY, et al. Achieving both high conductivity and reliable high strength for W–Cu composite alloys using spherical initial powders. Vacuum 2020;181:106920. https://doi.org/10.1016/j.vacuum.2020.109620.
[43] Huang YT, Zhou XL, Hua NB, Que WM, Chen WZ. High temperature friction and wear behavior of tungsten – copper alloys. Int J Refract Metals Hard Mater 2018;77:105–12. https://doi.org/10.1016/j.ijrmhm.2018.08.001.
[44] Han TL, Hou C, Zhao Z, Huang XT, Tang FW, Li YR, et al. W–Cu composites with excellent comprehensive properties. Compos B Eng 2022;233:109664. https://doi.org/10.1016/j.compositesb.2022.109664.
[45] Peng KF, Pan H, Zheng ZJ, Yu JL. Compaction behavior and densification mechanisms of Cu-W composite powders. Powder Technol 2021;382:478–90. https://doi.org/10.1016/j.powtec.2021.01.013.

[46] Wang C, Liang SH, Cao F, Zhang Q. Interface microstructure evolution of a novel CuW/Al composite fabricated by an infiltration method. J Alloys Compd 2020;816:152506. https://doi.org/10.1016/j.jallcom.2019.152506.
[47] Hiraoka Y, Hanado H, Inoue T. Deformation behavior at room temperature of W–80vol%Cu composite. Int J Refract Metals Hard Mater 2004;22(2–3):87–93. https://doi.org/10.1016/j.ijrmhm.2004.01.002.
[48] Zhang YJ, Song B, Zhao X, Shi YS. Microstructure and properties of Ag/SnO_2 functional material manufactured by selective laser melting. Nano Mater Sci 2019;1(3):208–14. https://doi.org/10.1016/j.nanoms.2019.04.001.
[49] Yang P, You X, Yi JH, Fang D, Bao R, Shen T, et al. Simultaneous achievement of high strength, excellent ductility, and good electrical conductivity in carbon nanotube/copper composites. J Alloys Compd 2018;752:431–9. https://doi.org/10.1016/j.jallcom.2018.03.341.
[50] Salvo C, Mangalaraja RV, Udayabashkar R, Lopez M, Aguilar C. Enhanced mechanical and electrical properties of novel graphene reinforced copper matrix composites. J Alloys Compd 2019;777:309–16. https://doi.org/10.1016/j.jallcom.2018.10.357.
[51] Ma B, Hishinuma Y, Shimada Y, Noto H, Kasada R, Oono N, et al. The size dependence of microstructure and hardness on the MA powders for the MA-HIP processed Cu-Y_2O_3 dispersion-strengthened alloys. Nucl Mater and Energy 2020;24:100773. https://doi.org/10.1016/j.nme.2020.100773.
[52] Liu S, Li LH, Zhou M, Liang SL, Zhang Y, Huang JL, et al. Preparation and properties of graphene reinforced Cu/0.5CeO230Cr electrical contact materials. Vacuum 2022;195:110687. https://doi.org/10.1016/j.vacuum.2021.110687.
[53] Li HY, Wang XH, Liu YF, Guo XH. Effect of strengthening phase on material transfer behavior of Ag-based contact materials under different voltages. Vacuum 2017;135:55–65. https://doi.org/10.1016/j.vacuum.2016.10.031.
[54] Chen ZK, Sawa K. Particle sputtering and deposition mechanism for material transfer in breaking arcs. J Appl Phys 1998;76:3326. https://doi.org/10.1063/1.358501.
[55] Bahramian A, Eyraud M, Maria S, Vacandio F, Djenizian T, Knauth P. Enhancing the corrosion resistance of Cu/Ni-P/Au electrical contacts by electropolymerized poly (methyl methacrylate). Corrosion Sci 2019;149:75–86. https://doi.org/10.1016/j.corsci.2018.12.026.